

Prospects for detection of spin accumulation using submicron planar Andreev array spectroscopy

F. Magnus, K. A. Yates, B. Morris, Y. Miyoshi, Y. Bugoslavsky, and L. F. Cohen^{a)}
Blackett Laboratory, Imperial College, Prince Consort Road, London SW7 2BZ, United Kingdom

G. Burnell and M. G. Blamire

Department of Materials Science and Metallurgy, University of Cambridge, Pembroke Street, Cambridge CB2 3QZ, United Kingdom

P. W. Josephs-Franks

National Physical Laboratory, Teddington, Middlesex TW11 0LW, United Kingdom

(Received 26 June 2006; accepted 21 November 2006; published online 27 December 2006)

Andreev spectroscopy can be employed to measure transport spin polarization. Planar Andreev devices have an advantage over point-contact Andreev spectroscopy as they offer greater control over interface quality and the possibility of spatially resolved information about spin polarization using submicron Andreev junction arrays. The authors compare the performance of Pb point contacts onto Cu and Co with that of large area and submicron planar junctions and singularly connected nanoarrays. Planar structures compare favorably to point contacts although the fabrication method influences extracted parameters. The authors find that submicron planar junction reproducibility does not adversely affect the prospects for developing arrays for detection of spin accumulation. © 2006 American Institute of Physics. [DOI: 10.1063/1.2424279]

Highly spatially resolved measurements of electron spin polarization are essential in order to study the influence of sample microstructure on the spin polarization and to quantify the spin diffusion and accumulation in nonmagnetic materials. Point-contact Andreev reflection¹ (PCAR) spectroscopy is a well established method for measuring the transport spin polarization in magnetic films.^{2,3} PCAR spectroscopy has the advantage of speed but the control of interfaces is extremely limited and the tip footprint is too large to achieve spatial resolution comparable to practical device length scales. Planar Andreev structures are one way to address these issues with arrays of junctions providing spatial resolution of spin polarization.

Planar Andreev nanojunctions have been made from SiN membrane technology,^{3,4} but these are difficult to scale up to produce array structures, although recent advances have shown that it is possible to control nanopore size from 1 to 30 nm through a SiN membrane using a focused ion beam method.⁵ Nanoscale junctions have also been achieved with planar thin-film edge contacts,⁶ but again this technique would not be well suited for array structures. Semiconductor device fabrication techniques have been used in the past to produce isolated submicron junctions but have not interrogated spin accumulation.⁷ Here we demonstrate the feasibility of deep submicron Andreev arrays on Cu and Co and compare the performance of planar structures to PCAR results. We examine the prospects of using this method to measure spin accumulation in both metals and semiconductors such as InAs, which is an important material for hybrid spintronics.⁸

The point contacts were made by pressing a mechanically sharpened Pb tip to the sample surface, as reported elsewhere.^{9,10} Planar contacts were fabricated onto Cu and Co using either conventional photolithography and microfab-

rication techniques or a combination of conventional techniques and focused ion beam (FIB) processing. In both cases, 50 nm thick films of Cu or Co were grown on thermally oxidized silicon substrates by dc magnetron sputtering. Following the deposition, a 50 μm wide track was defined using photolithography and broad-beam Ar⁺ ion milling. A set of superconducting lead tracks, 50 μm wide, crossing the Cu or Co track, was defined using a photolithographic liftoff process. For submicron planar contacts, the Cu or Co track was first covered with SiO_x in which apertures were opened with a FIB to define a reduced contact area. In the array structure, all the nanojunctions were connected to a single top contact (see inset of Fig. 2). The differential conductance of the junctions was measured using standard lock-in techniques.

The Andreev spectra are analyzed by finding the best least-squares fit to the generalized¹¹ Blonder-Tinkham-Klapwijk (BTK) theory,¹² in either the ballistic or diffusive regime. There are four fitting parameters: the superconductor energy gap Δ , the spin polarization P , a generic spectral broadening ω , and the dimensionless effective barrier parameter Z , which has been shown to be a reasonable approximation of the complex underlying physics of the interface.¹³ In the case where the full four-parameter fit is not unique, the polarization can be fixed at a certain value, P_{trial} , and a three-parameter fit performed (which is always unique). This process results in a one-dimensional function $\chi^2(P_{\text{trial}})$ where χ^2 is the sum of squared deviations and can be interpreted as the quality of the fit. This function should have a minimum at the correct value of P (see Ref. 9 for more details). The point-contact data only fit well to the ballistic regime, suggesting that the contacts are in fact a collection of much smaller actual point junctions.⁹

We compare the results from various planar samples: Pb/Cu and Pb/Co single junctions with a nominal area of $50 \times 50 \mu\text{m}^2$, single Pb/Cu junctions of size $500 \times 500 \text{ nm}^2$, and a Pb/Cu sample composed of an 8×8 array of $100 \times 100 \text{ nm}^2$ area junctions sharing a single top contact (see

^{a)}Electronic mail: l.cohen@imperial.ac.uk

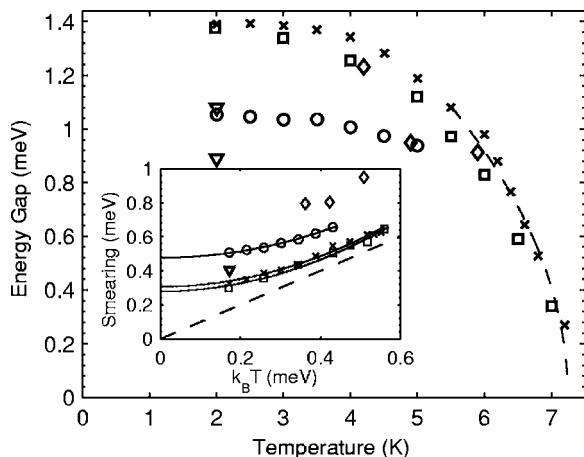


FIG. 1. Evolution of BTK fitting parameters with temperature. The main graph shows the energy gap Δ , including a fit to $(1-T/T_C)^{1/2}$ at $T \approx T_C$ for the planar $50 \mu\text{m}$ Cu junction. The theoretical value for Pb is 1.29 meV. Inset: The smearing parameter ω including parabolic fits to the data. The dashed line represents thermal broadening, where $\omega = k_B T$. Squares: Pb/Co $50 \mu\text{m}$ planar ($Z=0.27$ and $P=0.37$). Crosses: Pb/Cu $50 \mu\text{m}$ planar ($Z=0.50$ and $P=0$). Circles: Pb/Cu 100 nm planar array ($Z=0.27$ and $P=0$). Down triangles: Two Pb/Cu 500 nm planar samples ($Z=0.56$ and $P=0$). Diamonds: Pb/Cu point contact ($Z=0.22$ and $P=0.02$).

inset of Fig. 2 for a schematic cross section). The results from the array structure represent the average properties of the entire array. Point-contact measurements have been carried out on the contact pads of these samples.

Figure 1 shows the evolution of the energy gap and smearing fitting parameters with temperature. The large junctions and the array show the expected energy gap BCS temperature dependence. The Δ value at low temperature for the large junctions is close to the theoretical value for Pb (within experimental error), but the submicron single junctions and the array show significantly reduced Δ values with a spread of 10% between them. As all the submicron junctions are made using a FIB milling step, this suggests that the parameters are strongly influenced by the fabrication route. Reduced gap values have been reported previously from Andreev measurements and can be due to the suppression of Δ in a proximity induced superconducting layer at the interface.^{7,14}

The smearing parameter (inset) includes the combined effects of nonthermal and thermal broadening. At higher temperatures, thermal broadening is the dominant mechanism and the temperature dependence should be linear, as $\omega \approx k_B T$. The offset from this line is due to nonthermal effects, which become more significant at low temperatures. We would therefore expect the smearing to diverge from the linear dependence and to be nonzero at 0 K. This is approximated by a polynomial at low temperature and is in good agreement with the data. Several mechanisms could be responsible for the nonthermal broadening such as finite quasiparticle lifetime in the superconductor,¹⁵ interface scattering,⁹ or gap anisotropy over the junction area or across the junction.^{14,15} The submicron junctions show higher smearing than the large junctions due to FIB damage to the interface, and the array shows the highest smearing, most likely as a result of averaging over the 64 junctions. In general, however, we find that the planar structures yield lower values of smearing than point contacts.

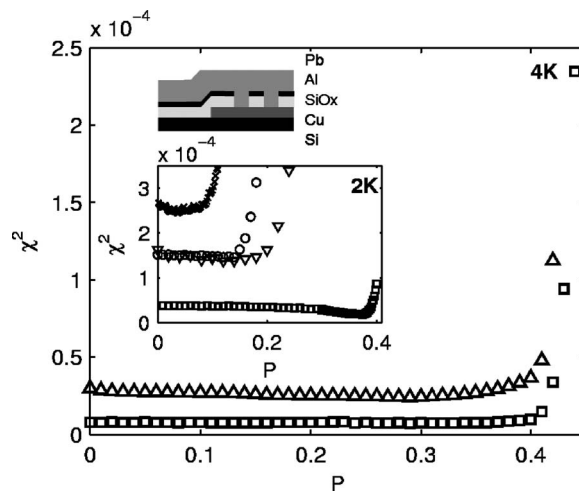


FIG. 2. Results of the $\chi^2(P)$ analysis. Main graph: Planar and point-contact junctions at 4 and 4.2 K, respectively. Insets: Planar samples at 2 K and a schematic cross section showing a part of the planar array of nanojunctions connected by a single top contact. Up triangles: Pb/Co point contact. Other symbols as in Fig. 1.

Figure 2 presents the $\chi^2(P)$ vs P results for planar junctions at 2 and 4 K. All samples show a relatively flat region at low P until a threshold value is reached above which the fit rapidly breaks down. The flat region is due to a compensation effect inherent in the fitting procedure, where the model is able to adjust Z to compensate for P . However, materials with finite polarization can produce a distinct minimum in the $\chi^2(P)$ dependence, as demonstrated in the inset, with the Co yielding a polarization of $P=0.37$. The main graph compares the results for planar and point-contact Co junctions at 4 and 4.2 K, respectively. The $\chi^2(P)$ dependence is much broadened at higher temperatures, and point-contact data are slightly broader than planar data, both consistent with the higher smearing. Neither the point contact nor the planar array correctly predicts $P=0$ for Cu from this fitting analysis and, while the threshold is sharper, the 100 nm array structure predicts P less accurately. It is clear that the $\chi^2(P)$ dependence is governed by a complex interplay between Z and ω and by minimizing ω , while retaining a finite Z is key to extracting P accurately.

A variation in the underlying properties between individual junctions of an array is, of course, undesirable and may increase the error in determining the spatial decay of spin polarization. Without access to each junction in the array we cannot discuss the spread of properties across all the 64 junctions. However, the $\chi^2(P)$ dependence of the single Pb/Cu 500 nm planar junction in the inset of Fig. 2 shows a similar behavior to that of the 100 nm array of junctions, suggesting that the average properties that we have measured for the 100 nm array are a good reflection of the performance of individual junctions within the array. Furthermore, the parameters of the submicron single junctions and the array vary by less than 20%.

All the planar structures we have studied have low smearing, and together with the improved fitting routine it is clear that we can differentiate between $P=0$ and finite P . Potentially, Andreev array structures could be used to study the spatial decay of the spin accumulation in Cu with a Co injector.¹⁶ To quantify the viability of this experiment we generate theoretical curves at a range of P and fit them using

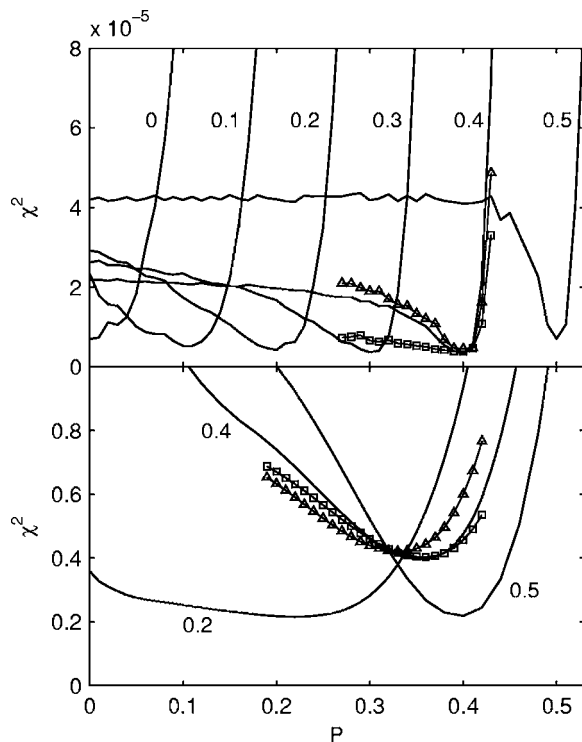


FIG. 3. Results of the $\chi^2(P)$ analysis for theoretical BTK curves for different parameter regimes. The labels indicate the polarization of the simulated spectra. Up triangles and squares represent a 20% increase in Z and ω , respectively, for the $P=0.4$ simulated spectrum. (a) Low Z and ω regimes, with parameters similar to the ones obtained for the $50 \times 50 \mu\text{m}^2$ planar junctions ($Z=0.27$ and $\omega=0.30$ meV). (b) High Z and ω regimes, with parameters chosen to resemble a superconductor/semiconductor interface ($Z=3.85$ and $\omega=0.58$ meV).

the method described above. Figure 3(a) shows the results for the spectra generated using parameters similar to the $50 \mu\text{m}$ planar junctions (i.e., the low Z and low ω regimes). The $\chi^2(P)$ curves have clearly resolved minima at the correct values of P , and interestingly the minima becomes sharper for higher polarizations. At low polarizations we should be able to distinguish between differences of 0.05, whereas for higher polarizations it should be possible to resolve variations in polarization as low as 0.01. The figure also shows the effect of a 20% variation in junction parameters on the $P=0.4$ simulated spectrum, as might be expected for array structures. A small increase in Z yields a sharper minimum, whereas increased smearing results in broadening of the minimum. In either case the threshold point is sharp, and clearly the 20% variability in parameters, although changing the shape of the $\chi^2(P)$ curve, does not adversely affect the accuracy of the extracted P value.

Taking this one step further, Fig. 3(b) presents the results for generated spectra with parameters chosen to resemble a superconducting-semiconducting (S-Sm) interface^{14,17} (i.e., high Z and ω). High Z is to be expected because of the Fermi velocity mismatch¹⁸ as well as the damage during processing which can also translate into higher effective smearing.¹⁴ The figure shows that in this regime the resolution of P is significantly reduced. However, it is still possible to differentiate between $P=0$ and polarizations of approximately 0.3 and above, and the resolution improves with increasing P . The influence of a 20% variation in junction parameters on the precision of extracted P is again shown for the $P=0.4$ curve. In this case, an increase in Z shifts the minimum from P

$=0.36$ down to $P=0.34$ (a change of approximately 6%), whereas increased smearing slightly broadens the minimum but does not affect P . So the extracted P value can be influenced by junction variability, placing tighter requirements on junction reproducibility for S-Sm junctions, but our present reproducibility statistics suggest that this is not overly detrimental. Indeed, the parameter set we have used in Fig. 3(b) represents a “worst case scenario” where we have used $Z=3.85$, whereas the lower bound for Pb/InAs junctions based on the Fermi velocity mismatch gives a $Z=0.95$.

To summarize, we present results demonstrating that the manufacture of submicron planar Andreev structures using a FIB route is feasible. Although junction properties are affected by this type of processing, the resulting parameters are suitable for the measurement of spin accumulation and diffusion in metallic spintronic devices of, for example, the Jedema *et al.* type.¹⁶ Results from simulated spectra indicate that it should be feasible to detect spin accumulation in a semiconductor, with resolution of the order of $P=0.1$ only for $P \geq 0.3$ and then only in the case where underlying junction properties are tightly controlled. It is also important to minimize the interface barrier and sources of smearing to increase the resolution of P , particularly if the technique is to be used to study spin accumulation in semiconductors.

This work was supported by the U.K. Engineering and Physical Sciences Research Council Grant Nos. GR/T03802 and EPC511972 and the National Physical Laboratory under the DTI Quantum Metrology Programme.

¹A. F. Andreev, Zh. Eksp. Teor. Fiz. **46**, 1823 (1964) [Sov. Phys. JETP **19**, 1228 (1964)].

²R. J. Soulen, J. M. Byers, M. S. Osofsky, B. Nadgorny, T. Ambrose, S. F. Cheng, P. R. Broussard, C. T. Tanaka, J. Nowak, J. S. Moodera, A. Barry, and J. M. D. Coey, Science **282**, 85 (1998).

³S. K. Upadhyay, R. N. Louie, and R. A. Buhrman, Appl. Phys. Lett. **74**, 3881 (1999).

⁴D. C. Ralph, C. T. Black, and M. Tinkham, Phys. Rev. Lett. **74**, 3241 (1995).

⁵H. X. Wei, R. M. Langford, X. F. Han, and J. M. D. Coey, J. Appl. Phys. **99**, 08C501 (2006); H. X. Wei, T. X. Wang, E. Clifford, R. M. Langford, X. F. Han, and J. M. D. Coey, *ibid.* **99**, 08C512 (2006).

⁶O. Cespedes, E. Clifford, and J. M. D. Coey, J. Magn. Magn. Mater. **290**, 113 (2005).

⁷M. Jakob, H. Stahl, J. Knoch, J. Appenzeller, B. Lengeler, H. Hardtdegen, and H. Luth, Appl. Phys. Lett. **76**, 1152 (2000).

⁸B. N. Murdin, K. Litvinenko, J. Allam, C. R. Pidgeon, M. Bird, K. Morrison, T. Zhang, S. K. Clowes, W. R. Branford, J. Harris, and L. F. Cohen, Phys. Rev. B **72**, 085346 (2005).

⁹Y. Bugoslavsky, Y. Miyoshi, S. K. Clowes, W. R. Branford, M. Lake, I. Brown, A. D. Caplin, and L. F. Cohen, Phys. Rev. B **71**, 104523 (2005).

¹⁰S. K. Clowes, Y. Miyoshi, Y. Bugoslavsky, W. R. Branford, C. Grigorescu, S. A. Manea, O. Monnereau, and L. F. Cohen, Phys. Rev. B **69**, 214425 (2004).

¹¹I. I. Mazin, A. A. Golubov, and B. Nadgorny, J. Appl. Phys. **89**, 7576 (2001).

¹²G. E. Blonder, M. Tinkham, and T. M. Klapwijk, Phys. Rev. B **25**, 4515 (1982).

¹³K. Xia, P. J. Kelly, G. E. W. Bauer, and I. Turek, Phys. Rev. Lett. **89**, 166603 (2002).

¹⁴K. Neurohr, A. A. Golubov, T. Klocke, J. Kaufmann, T. Schapers, J. Appenzeller, D. Uhlisch, A. V. Ustinov, M. Hollfelder, H. Luth, and A. I. Braginski, Phys. Rev. B **54**, 17018 (1996).

¹⁵Y. de Wilde, T. M. Klapwijk, A. G. M. Jansen, J. Heil, and P. Wyder, Physica B **218**, 165 (1996).

¹⁶F. J. Jedema, A. T. Filip, and B. J. van Wees, Nature (London) **410**, 345 (2001).

¹⁷A. W. Kleinsasser, T. N. Jackson, D. McInturff, F. Rammo, G. D. Pettit, and J. M. Woodall, Appl. Phys. Lett. **57**, 1811 (1990).

¹⁸I. Zutic and O. T. Valls, Phys. Rev. B **61**, 1555 (2000).